Heavily Ce^{3+}-doped phosphate glass scintillator for X-ray detection

XIAOYUN XU[1,2,*], XINYUE CHEN[1], XINYI LIU[1], YIFAN CAO[2]
[1]*Guangzhou City University of Technology, Guangzhou 510800, China*
[2]*State Key Laboratory of Luminescent Materials and Devices, South China University of Technology, Guangzhou 510640, China*

The scintillator is the key material for various applications fields such as high-energy physics, nuclear medical imaging, and environmental monitoring. Despite of the great success in construction of various inorganic scintillators, the fabrication of the candidate with high active dopant solubility remains a great challenge. In this manuscript, we report a scintillating phosphate glass with extremely high Ce solubility of more than 20 mol%. It exhibits excellent radiation response properties not only to X-ray but also alpha particle. In addition, the material shows fast decay dynamics with the lifetime of 31ns. Furthermore, the materials also exhibit strong radiation stability and the continuous radiation exposure does not lead to obvious degradation. By using this material, their practical applications for X-ray imaging have been demonstrated. The results demonstrate that the Ce-doped phosphate glass show great promise for high-energy radiation detection.

(Received June 3, 2025; accepted October 10, 2025)

Keywords: Scintillator, Rare earths, Glass, Luminescence, Radiation detection

1. Introduction

The scintillator, which functionalizes to convert high-energy radiation into low energy photons, have demonstrated unique advantages in various applications fields such as high-energy physics, nuclear medical imaging, and environmental monitoring [1-5].

Compared with the traditional crystalline scintillators, glass host exhibits distinctive characteristics including excellent optical quality, low cost, and ease of fabricating complex geometries, making them a research hotspot in the radiation detection field. In the past several years, significant progress has been achieved in developing novel glass scintillators [6-10].

Pr^{3+}-doped lithium glass with ultra-fast decay lifetime of 6 ns for alpha particle and neutron has been proposed and its application for laser fusion experiments at the GEKKO XII facility have been explored [11]. Novel superdense Ce^{3+}-activated lutetium silicate scintillating glass with the density of 7.15 g/cm^3 has been designed and fabricated. This represents the highest density among the fast decay glass system and the excellent X-ray radiation detection performance has been demonstrated [12]. Glass materials also exhibit reliable fibrilization performance, enabling the fabrication of various scintillating glass fibers. The novel radiation detectors based on these scintillating fibers can achieve higher spatial resolution imaging and remote neutron flux monitoring [13-15].

In addition, the functionalization of glass via controllable crystallization toward glass composite scintillator have also been tried and the efficient neutron detection, X-ray imaging and ray-neutron discrimination have been achieved [16-19]. All above results indicate that the scintillating dopants, generally Ce^{3+} and Eu^{2+}, govern the performance of the material. Particularly, the solubility of active dopants directly governs the scintillating yield. Despite of great progress have been achieved, the dopant concentration is usually limited to be ~1 mol% [20]. The way to improve the dopant solubility remains a long-standing challenge.

In this paper, we report on the design and fabrication of novel scintillating phosphate glass with extremely high Ce solubility of more than 20 mol%. The X-ray and alpha scintillating properties have been studied and the samples exhibit excellent radiation response performance. In addition, the materials also exhibit strong radiation stability. Furthermore, their piratical applications for X-ray imaging have been demonstrated. The materials are believed to show great potentials for high-energy radiation detection.

2. Experimental section

2.1. Material synthesis

Ce-doped phosphate glasses composed of La_2O_3-P_2O_5-CeO_2 with different mole ratio was designed, as presented in Table 1. The glass samples were synthesized using the classic melt-quenching method. High-purity precursors (La_2O_3, $(NH_4)H_2PO_4$ and CeO_2) were fully mixed in mortar. In a typical synthesis process, about 30 g of the raw materials was transferred into a corundum crucible and melted at 1350 °C for 30 minutes in a muffle furnace. The homogeneous melt was rapidly quenched by pressed with a stainless-steel plate. The resultant glass with the thickness of ~3 mm was cut into 5×5 mm samples. The glass samples were then annealed at 450 °C for 6 hours. Finally, the samples were carefully polished for structural and optical characterization.

2.2. Material characterizations

The thermal properties of glass samples were characterized with a STA449C differential scanning calorimeter (DSC), with the heating rate of 10 °C/min at the standard air atmosphere. The compositions of the glass samples were studied through a Nova Nano SEM 430 scanning electron microscope (SEM) integrated with an energy dispersive spectrometer (EDS). The microstructure of the glass samples was analyzed by using the Raman scattering spectroscopy on a Raman spectrometer (Renishaw in via) equipped with the 532 and 785 nm laser. Absorption spectra was recorded on a PerkinElmer Lambda 900 UV-Vis-NIR spectrophotometer. The photoluminescence spectrum and decay dynamics were measured on the Edinburgh FLS 920 spectrofluorometer with an xenon lamp as the excitation source and PMT as the detector. The complete scintillation detection system consists of glass composite materials, a photomultiplier tube (PMT), a high-voltage power supply, a multichannel analyzer (MCA), and a computer. In this system, the glass composite material interacts with high-energy particles, releasing low-energy photons. These photons are then detected and amplified by the photomultiplier tube. Finally, the amplified signals from the PMT are acquired by the multichannel analyzer, and the results are displayed on the computer. This sophisticated experimental device enables precise quantification of the sample's light yield. The scintillating luminescence was characterized by employing a Mini-X-OEM X-ray tube (Amptek Inc.) as the excitation source. The corresponding spectrum was recorded with an Ocean Maya 2000 Pro spectrometer (Ocean Optics).

3. Results and discussion

The chemical compositions of the glass system are summarized in Table 1. The dopant concentration of CeO_2 was controlled from 4 to 22 mol%. The total content of CeO_2 and La_2O_3 was set to be 25%. Energy dispersive spectroscopy (EDS) analysis was performed on a typical sample G and the result is shown in Fig. 1(a). It can be observed that the sample is composed of La, P, Ce and O. The structure of the samples was characterized by Raman scattering. As shown in Fig. 1(b), the characteristic peak observed at 700 cm^{-1} can be ascribed to the P–O–P symmetric stretch of bridging oxygens connecting adjacent [PO_4] tetrahedral [21].

The results indicate the formation of phosphate components in the glass system. EDS mapping was performed and the results are presented in Figs. 1(c)-(f). It can be observed that the investigated elements are homogeneously distributed, confirming the success in fabrication of the sample with high quality.

Table 1. The compositions of the glass samples

Sample	Composition (mol%)		
	La_2O_3	P_2O_5	CeO_2
A	21	75	4
B	19	75	6
C	17	75	8
D	15	75	10
E	11	75	14
F	7	75	18
G	3	75	22

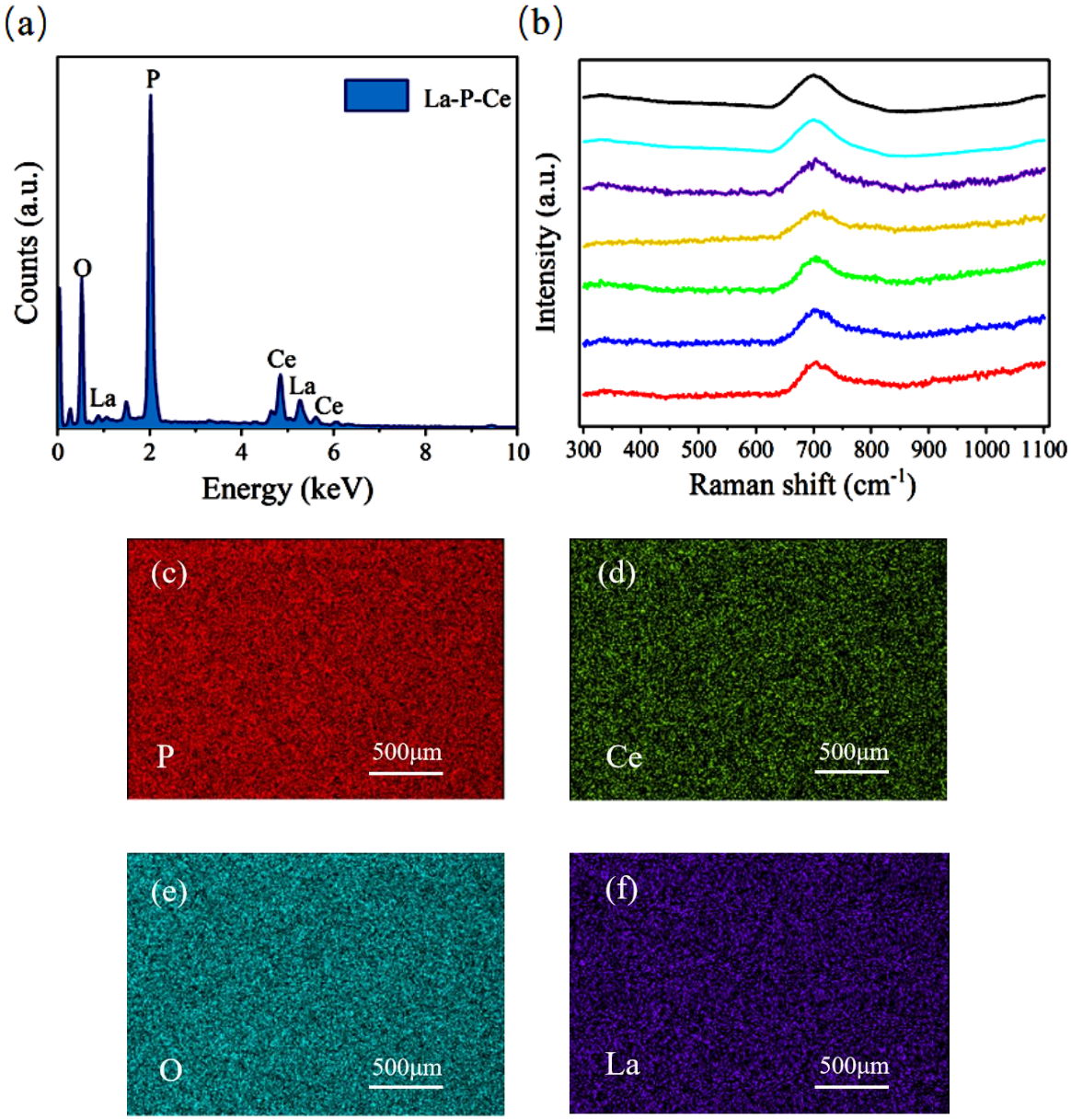

Fig. 1. Structure analysis of Ce-doped glasses. a) EDS analysis on the glass sample. (b) Raman scattering spectra of the glass samples.(c-f) The element mapping of various elements of P, Ce, La and O (colour online)

The optical properties of various Ce-doped glass samples were studied. Fig. 2(a) exhibit the optical transmission spectra of the samples with various Ce^{3+} doping concentration. All of the samples exhibit transmission large than 60% in the visible waveband, indicating the excellent optical quality. Fig. 2(b) shows the emission spectra under excitation with 320 nm. The broadband characteristic emission bands covering from 340 nm to 450 nm can be observed and they can be indexed to the $5d^1 \rightarrow {}^2F_{5/2,7/2}$ transitions of Ce^{3+} [22]. Fig. 2(c) presents the excitation spectra of samples by monitoring the emission at 350 nm. The broadband excitation bands from 200 to 340 nm can be observed and they can be ascribed to the electronic transitions from the 4f ground states to the 5d excited states of Ce^{3+} [22]. The optimal excitation and emission occurs at the sample with 14 mol% Ce^{3+}. Notably, no obvious decrease in the excitation and emission intensity with further increase of the Ce^{3+} doping concentration. The results demonstrate that the concentration quenching can be well prevented and the dopant solubility is rather high in the investigated glass system. The luminescence decay dynamics was studied and the decay curves of the emission at 350 nm are summarized in Fig. 2(d). They can be fitted to the single-exponential function and the characteristic decay lifetime is calculated to be around 31 ns. The short decay process indicates the great potential for scintillating application.

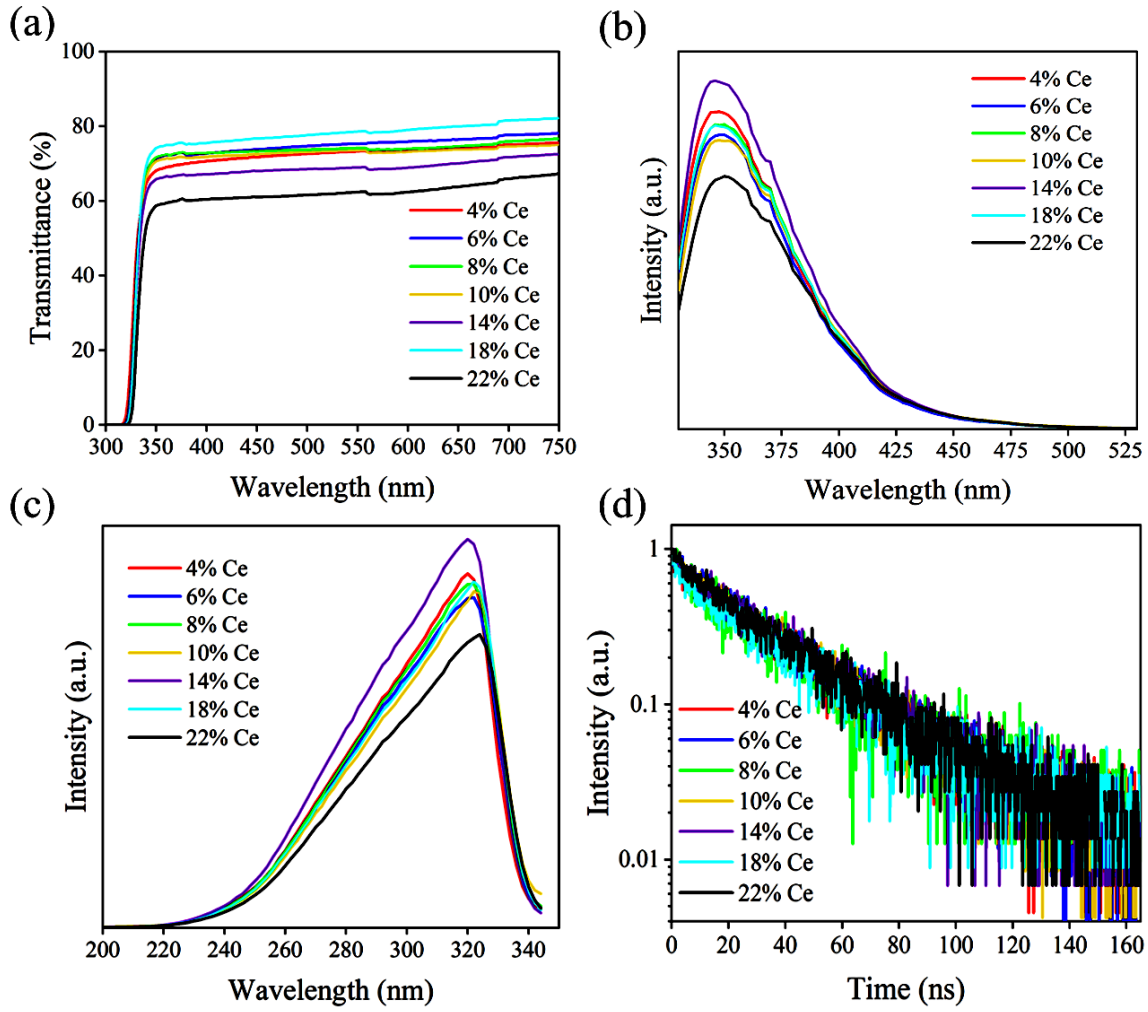

Fig. 2. Optical properties of Ce-doped glasses. (a) Absorption spectra glass samples. (b) The luminescence spectra upon excitation with 320 nm. (c) The excitation spectra of glass samples by monitoring the emission at around 350 nm. (d) The luminescence decay curves with luminescence at 350 nm (colour online)

The scintillating properties of Ce-doped glass samples were studied. Fig. 3(a) presents the interaction mechanism between the X-ray and the glass. Under the excitation with high-energy X-ray, many hot electrons and holes can be generated through the photoelectric effect or Compton effect inside the material. Some of the carriers will be trapped by the deep traps and most of them transfer through the lattice. They will finally recombine in the active Ce^{3+} dopant, resulting in the scintillating emission. The absorption coefficient of the glass was calculated and the standard BGO sample is also shown for comparison. As shown in Fig. 3(b), the sharp peaks at 0.006, 0.040 KeV can be ascribed to the Ce_{L2} and Ce_K, respectively. The total absorption coefficient of the studied glass is relatively higher compared with the that of the BGO. The X-ray induced luminescence was characterized and shown in Fig. 3(c). The intense emission with the central wavelength at ~350 nm can be observed, consistent with the ultraviolet light induced luminescence feature.

The scintillating properties under excitation with alpha particle were studied. Fig. 3(d) show the pulse height spectra of the fabricated sample and the standard lithium glass. In this study, ^{241}Am radioactive source was used as the alpha particles produced by the ^{6}Li(n, alpha)^{3}H reaction and the energy is estimated to be 5.5 MeV. The detected signal peak is located at ~365 channels. The signal peak of the commercial lithium glass under the same conditions is at ~856 channels. Thus, the light output of the sample under alpha particle excitation is about 42.6% of the standard sample. Ce dopant concentration dependent channel number of the signal peak is summarized and exhibited in Fig. 3(e). It can be observed that the channel number increases with the enhancement of Ce concentration. No obvious saturation can be observed even when the Ce concentration reaches to 22 mol%, indicating the success in suppression of quenching phenomenon in the glass.

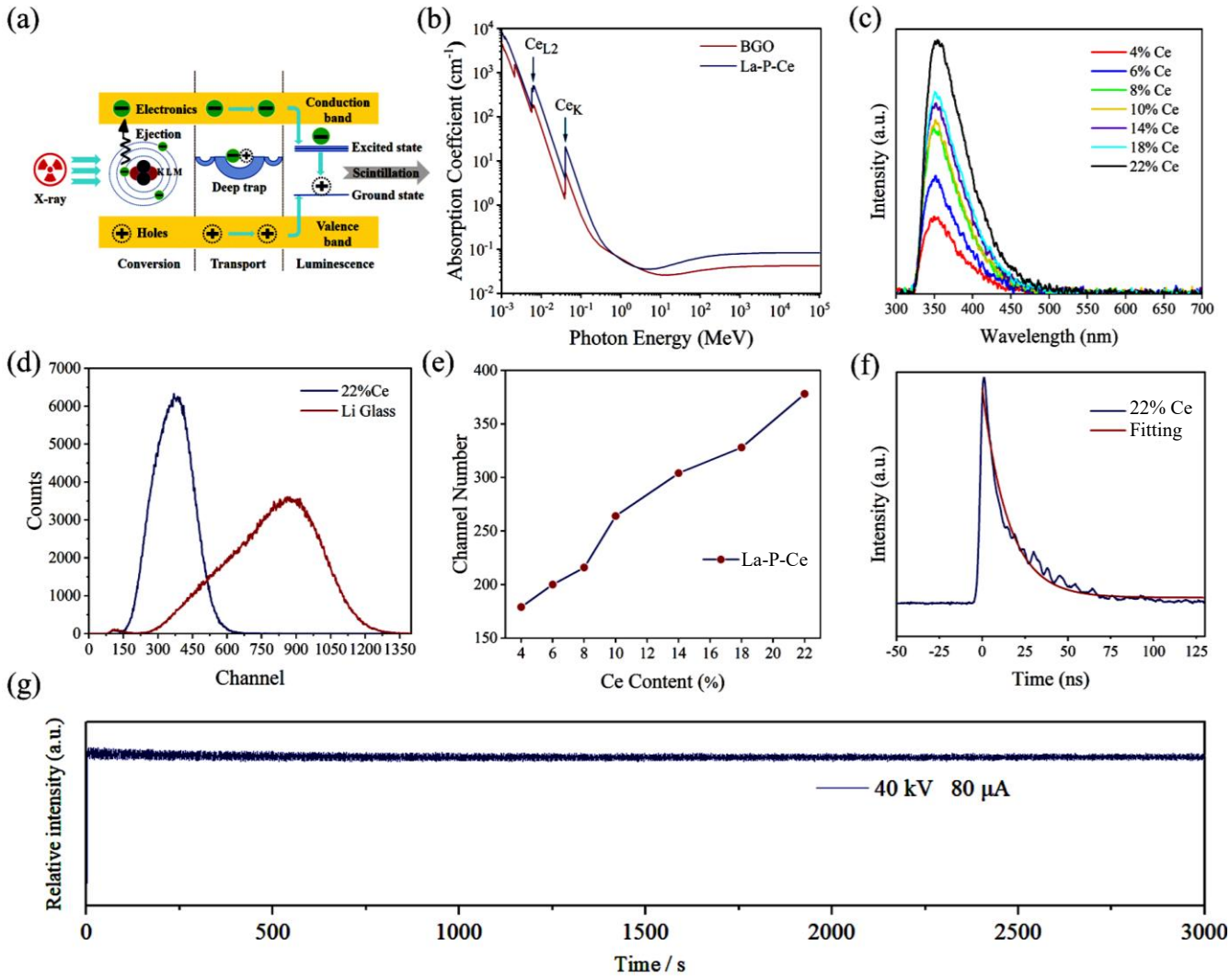

Fig. 3. Scintillating properties of Ce-doped glasses. (a) The scintillating mechanism of the X-ray induced emission. (b) The comparison on the X-ray absorption coefficient of BGO and glass samples. (c) The X-ray induced luminescence spectra. (d) The scintillating response under excitation with alpha particle. The standard GS20 sample is also shown for comparison. (e) Ce concentration dependent scintillating performance under excitation with alpha particle. (f) The single pulse signal of the glass under excitation with alpha particle. (g) The scintillating emission intensity evolution in the time window of 50 minutes (colour online)

The decay dynamics under excitation with alpha particle was studied and the monitored decay curve is exhibited in Fig. 3(f). The decay process is fast and it implies the great promise for dynamic event monitoring. Furthermore, the radiation stability of the glass sample was studied. Fig. 3(g) exhibits the scintillating emission intensity evolution with the radiation duration of 50 minutes. No obvious radiation induced emission degradation can be observed, demonstrating the excellent radiation hardness of the fabricated glass samples.

The attractive scintillating properties of the fabricated glass samples prompt us to explore their application for X-ray imaging. In this study, the typical sample with the Ce concentration of 22 mol% was used. Fig. 4(a) illustrates the principle of X-ray imaging system. It consists of an X-ray source, the glass sample as the scintillation screen, the imaging object, and a CMOS camera. The imaging target was placed between the X-ray source and the scintillation screen. The X-ray radiation first passes through the target and then arrives at the scintillation screen. The microscopic information of the target mediated by the scintillating emission can be captured by using the CMOS camera. The modulation transfer function (MTF) obtained by the slanted-edge approach is shown in Fig. 4(b). The spatial resolution was estimated to be 18 lp/mm. The imaging resolution can also be characterized by using the X-ray line-pair card. Fig. 4(c) and (d) exhibit the used standard X-ray line-pair card and the test result, respectively. The corresponding imaging resolution was estimated to be 18 lp/mm, well consistent with the MTF result. The imaging system was further employed for imaging of metal

pattern and circuit board. Figs. 4(e) and (f) exhibit the metal patterns used for imaging and the corresponding X-ray imaging picture, respectively. Figs. 4(g) and (h) show the circuit board employed for imaging and the corresponding X-ray imaging images, respectively. Notably, the microscopic and the internal structure of the imaging targets can be clearly distinguished.

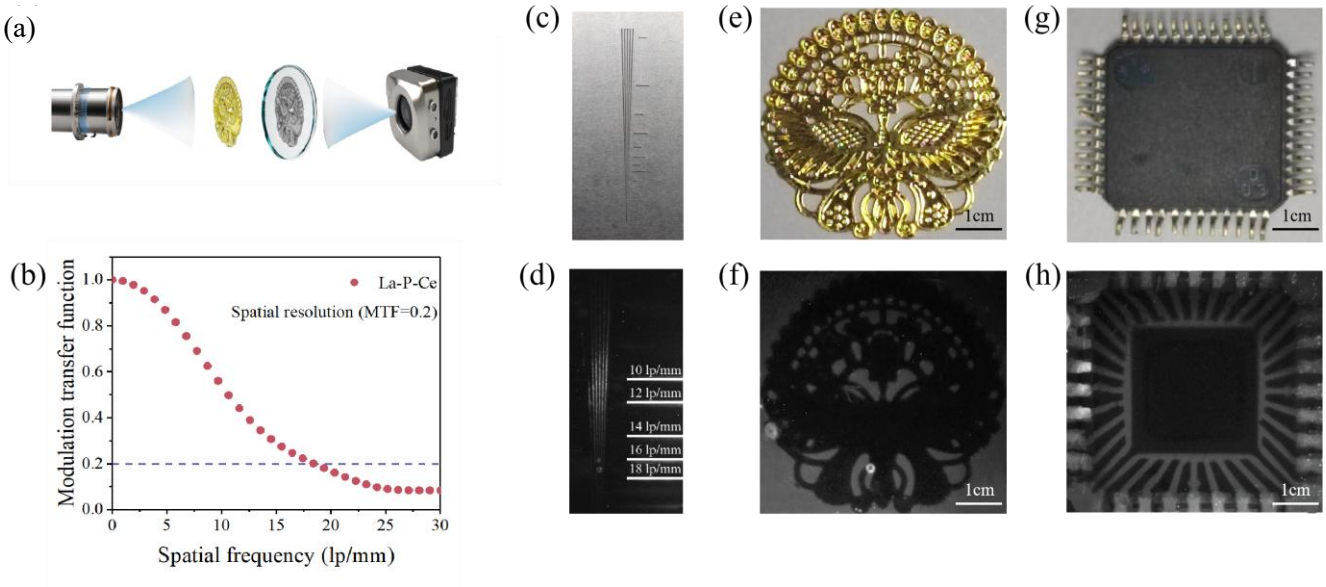

Fig. 4. X-ray imaging application of Ce-doped glasses. (a) Schematical illustration of the principle for X-ray imaging. (b) MTF of X-ray imaging images by using the glass sample. (c, d) The standard X-ray imaging line-pair card (c) and the corresponding imaging images (d). (e, f) The metal patterns used for image (e) and the corresponding X-ray imaging images (f). (g, h) Circuit board (g) and the corresponding X-ray imaging pictures (h) (colour online)

4. Conclusions

In this manuscript, we have proposed a scintillating phosphate glass system with high Ce solubility more than 20 mol%. The optical, X-ray and alpha scintillating properties have been studied and the samples exhibit excellent radiation response performance.

Interestingly, the materials also show strong radiation stability and no obvious degradation has been observed even after long-duration high-energy radiation. The practical applications for X-ray imaging on the metal patterns and circuit board have been demonstrated. The results not only prove the excellent potential of heavily doped glass materials for high-energy imaging, but also provide useful reference for active photonics such as optical amplification and laser generation.

Acknowledgments

This study was supported by the National Natural Science Foundation of China (No. 12104163), the Department of Education of Guangdong Province (2024KTSCX156), College Students' Innovation and Entrepreneurship Training Program (No. J3124174) and the Open Research Fund of State Key Laboratory of Luminescent Materials and Devices, South China University of Technology (2025-skllmd-21).

References

[1] Q. Chen, J. Wu, X. Ou, B. Huang, J. Almutlaq, A. A. Zhumekenov, X. Guan, S. Han, L. Liang, Z. Yi, J. Li, X. Xie, Y. Wang, Y. Li, D. Fan, D. B. L. Teh, A. H. All, O. F. Mohammed, O. M. Bakr, T. Wu, M. Bettinelli, H. Yang, W. Huang, X. Liu, Nature **561**(7721), 88 (2018).

[2] J.-X. Wang, O. Shekhah, O. M. Bakr, M. Eddaoudi, O. F. Mohammed, Chem **11**(1), 102273 (2025).

[3] S. Lv, D. Wang, J. Tang, Z. Liu, H. Inoue, B. Tang, Z Sun, L. Wondraczek, J. Qiu, S. Zhou, Nature Communications **15**(1), 6746 (2024).

[4] Z. Wang, C. Dujardin, M. S. Freeman, A. E. Gehring, J. F. Hunter, P. Lecoq, W. Liu, C. L. Melcher, C. L. Morris, M. Nikl, G Pilania, R. Pokharel, D. G. Robertson, D. J. Rutstrom, S. K. Sjue, A. S. Tremsin, S. A. Watson, B. W. Wiggins, N. M. Winch, M. Zhuravleva, IEEE Transactions on Nuclear Science **70**(7), 1244 (2023).

[5] T. J. Hajagos, C. Liu, N. J. Cherepy, Q. Pei, Advanced Materials **30**(27), 1706956 (2018).

[6] E. Kaewnuam, N. Wantana, J. Kaewkhao, H. J. Kim, Materials Today-Proceedings **17**(4), 1787 (2019).

[7] D. Zhang, S. Lin, M. Xia, Y. Rao, S. Qian, J. Ren, X. Zhang, Y. Xu, D. Chen, Laser & Photonics Reviews **19**(13), 2500354 (2025).

[8] C. Zhao, Y. Wang, S. Bao, Y. Zang, X. Liu, W. Huang, Advanced Materials **37**(21), 2500925 (2025).
[9] Z. Zheng, Y. Tong, R. Wei, F. Hu, X Sun, H. Guo, Journal of the American Ceramic Society **103**(4), 2548 (2020).
[10] D. Yang, K. Ge, H. Ban, X. Chu, S. Liu, S. Qian, Z. Hua, H. Cai, D. Chen, J. Jia, X. Sun, J. Ren, G. Tang, M. Zhang, J. Xiao, Y. Du, Ceramics International **50**(22), 47253 (2024).
[11] Y. Arikawa, K. Yamanoi, T. Nakazato, E. S. Estacio, T. Shimizu, N. Sarukura, M. Nakai, T. Norimatsu, H. Azechi, T. Murata, S. Fujino, H. Yoshida, K. Kamada, Y. Usuki, T. Suyama, A. Yoshikawa, N. Sato, H. Kan, Review of Scientific Instruments **80**(11), 113504 (2009).
[12] F. Zhang, D. Wang, G. Du, H. Li, D. Hou, Y. Qi, S. Lv, S. Zhou, Journal of Rare Earths **43**(10), 2137 (2024).
[13] S. Lv, J. Tang, J. Chen, P. Liu. J. Guo, Y. Ma, J. Qiu, S. Zhou, Advanced Materials Technologies **6**(1), 2000696 (2021).
[14] S. Lv, F. Zhang, X. Li, T. Jiang, Z. Yang. J. Li, H. Zhu, J. Guo, J. Qiu, S. Zhou, Advanced Optical Materials **12**(10), 2302306 (2024).
[15] H. Zhu, S. Lv, D. Hou, X. Li, F. Zhang, T. Jiang, Z. Yang, J. Li, S. Zhou, Y. Li, Laser & Photonics Reviews **19**(2), 2400582 (2024).
[16] J. Tang, S. Lv, Z. Lin, G. Du, M. Tang, X. Feng, J. Guo, X. Li, J. Chen, L. Wei, J. Qiu, S. Zhou, Journal of Materials Science & Technology **129**, 173 (2022).
[17] G. Du, S. Wen, J. Zhao, P. Ran, D. Wang, L. Wei, X. Qiao, Y. Yang, J. Qiu, S. Zhou, Advanced Materials **35**(11), 2205578 (2023).
[18] D. Wang, S. Zhang, J. Chen, D. Tu, S. Lv, Z. Wei, B. Tang, Z. Sun, J. Qiu, S. Zhou, Advanced Functional Materials **34**(36), 2401992 (2024).
[19] D. Wang, H. Li, J. Chen, D. Hou, X. Liu, Z. Yu, S. Lv, J. Qiu, S. Zhou, Advanced Materials **37**(1), 2412661 (2025).
[20]C. Canevali, M. Mattoni, F. Morazzoni, R. Scotti, M. Casu, A. Musinu, R. Krsmanovic, S. Polizzi, A. Speghini, M. Bettinelli, Journal of the American Chemical Society **127**(42), 14681 (2005).
[21] R. K. Brow, E. Metwalli, D. L. Sidebottom, Inorganic Optical Materials II. SPIE **4102**, 88 (2000).
[22] J. Bei, G. Qian, X. Liang, S. Yuan, Y. Yang, G. Chen, Materials Research Bulletin **42**(7), 1195 (2007).

*Corresponding author: xuxiaoyun@gcu.edu.cn